Materials Advances

ROYAL SOCIETY OF CHEMISTRY

PAPER

View Article Online
View Journal | View Issue

Check for updates

Cite this: *Mater. Adv.*, 2024, 5, 1552

# Efficient degradation of orange G dye using the quartz-sand@polythiophene composite for peroxymonosulfate activation: a sustainable approach for advanced oxidation processes†

Asma Amjlef, * Abdellah Ait El Fakir, Salaheddine Farsad, Aboubakr Ben Hamou, Ayoub Chaoui, Saïd Et-Taleb* and Noureddine El Alem

In this work, a composite material, QS@PTh, comprising quartz-sand (QS) and polythiophene (PTh) was used for the activation of peroxymonosulfate (PMS) to degrade Orange G dye (OG). The QS@PTh composite was synthesized through a polymerization process that resulted in the attachment of polythiophene onto the quartz-sand surface. The formation of QS@PTh was demonstrated using X-ray diffraction (XRD), scanning electron microscopy with energy-dispersive X-ray spectroscopy (SEM/EDX), and Fourier-transform infrared (FTIR) spectroscopy. The activation of PMS by the QS@PTh composite was evaluated through degradation experiments using Orange G dye as a model pollutant. The results demonstrated the efficient degradation of Orange G dye by the QS@PTh/PMS system, achieving a degradation efficiency of 99.5% and a COD removal of 79.4% within 60 min. The mechanism of PMS activation for OG degradation was suggested, highlighting the role of electron transfer from the polythiophene component to PMS, leading to the production of highly reactive species such as hydroxyl radicals ($^{\bullet}OH$), sulfate radicals ($SO_4^{\bullet-}$), and singlet oxygen ($^1O_2$). Furthermore, the system exhibited remarkable efficacy in degrading other organic pollutants and real water samples, confirming its feasibility for decontaminating various pollutants. These promising results position QS@PTh/PMS as a versatile solution with potential application in the industrial sector. Additionally, the QS@PTh composite's catalytic activity remained robust even after five cycles, indicating its potential for repeated use. These outcomes collectively underscore the utility of QS@PTh as a performant catalyst for PMS activation in the degradation of organic contaminants, showcasing its potential for environmental remediation applications.

Received 24th August 2023,
Accepted 10th December 2023

DOI: 10.1039/d3ma00596h

rsc.li/materials-advances

Open Access Article. Published on 11 December 2023. Downloaded on 2/8/2026 11:39:59 PM.
This article is licensed under a Creative Commons Attribution-NonCommercial 3.0 Unported Licence.

## 1. Introduction

Recently, the persistent contamination of water bodies with organic pollutants has become a significant environmental concern. Synthetic dyes released from industrial activities pose a threat to both aquatic ecosystems and human health.[1,2] Consequently, the development of effective and sustainable strategies for the removal of these contaminants is of paramount importance.[3–6] Peroxymonosulfate based advanced oxidation processes (AOPs) have emerged as a promising technique for the degradation of organic contaminants due to the versatility, longer half-life ($t_{1/2}$ = 30–40 μs), and strong oxidizing potential (2.5–3.1 V) of sulfate radicals.[7,8] The activation of PMS entails the generation of sulfate radicals ($SO_4^{\bullet-}$) by the breakdown of the O–O bond.[9] To activate PMS, various techniques have been employed, including radiation, alkaline conditions, electrochemical processes, thermal treatment, transition metal ions, and metal oxides.[10,11]

However, these activation methods typically necessitate high temperatures, extended reaction times, or the introduction of costly transition metal catalysts, which can have adverse environmental impacts.[12] To overcome these limitations, researchers have been exploring alternative catalysts that can activate PMS under ambient conditions, thereby enhancing the degradation efficiency of pollutants.

Carbocatalysts have gained a great deal of attention due to their biocompatibility, high catalytic activity, and eco-friendliness.[13] Additionally, they have been confirmed to effectively activate oxidants (peroxymonosulfate and persulfate (PS)) without causing secondary pollution.[14] Annamalai *et al.* reported that carbocatalysts, particularly those doped with heteroatoms such as nitrogen, phosphorus, and sulfur, have shown remarkable catalytic activity in activation.[15]

*Laboratory of Materials and Environment, Faculty of Sciences, Ibn Zohr University, Agadir, Morocco. E-mail: amjlef.asma@gmail.com, said.ke.ettaleb@gmail.com*

† Electronic supplementary information (ESI) available. See DOI: https://doi.org/10.1039/d3ma00596h



© 2024 The Author(s). Published by the Royal Society of Chemistry

Open Access Article. Published on 11 December 2023. Downloaded on 2/8/2026 11:39:59 PM. This article is licensed under a Creative Commons Attribution-NonCommercial 3.0 Unported Licence.

Traditionally, the use of N or S-doped carbon materials faced challenges related to the instability of nitrogen/sulfur doping,[16] resulting in the need for an energy-intensive pyrolysis process, which could lead to costly materials.[15] However, a groundbreaking facet of our research lies in the direct utilization of conductive materials featuring a conjugated system composed of alternating heteroatoms and carbon atoms, eliminating the need for pyrolysis. This approach holds the potential to yield cost-effective materials with superior catalytic capability. For example, Sun *et al.* confirmed that polyaniline exhibits superior catalytic performance compared to conventional metal-based catalysts and commonly used N-doped carbocatalysts in the degradation of methyl orange (MO).[13] Similarly, Ait El Fakir *et al.* demonstrated that hematite sand coated with nitrogen-rich polymers (polypyrrol and polyaniline) could effectively activate PS for the degradation of organic pollutants.[17]

Despite the extensive research on catalysts, there has been relatively limited exploration of sulfur-rich carbocatalysts. This gap in the literature underscores the need for further investigation in this area. In light of this, polythiophene, a sulfur-rich conductive polymer with a unique chemical structure, has been widely studied for its excellent electrical conductivity, and catalytic properties.[18,19] Its conjugated backbone, consisting of alternating sulfur and carbon atoms, provides a suitable platform for electron transfer reactions,[18,20] making it a promising catalyst for industrial applications. However, polythiophene alone still has some drawbacks for practical applications, including lack of selectivity, difficult separation, limited stability and poor mechanical strength.[21] In order to address these challenges, quartz-sand can be used as a carrier for polythiophene, offering several advantages for the activation of PMS, including enhanced catalytic activity, improved stability, good mechanical strength, and providing ease of separation of the catalyst from the mixture. The synergistic effects between polythiophene and the quartz sand substrate offer a sustainable and cost-effective solution for the degradation of organic contaminants in large-scale applications.

To the best of our knowledge, no prior research has been published regarding the use of polythiophene-coated quartz sand as a catalyst for activating PMS in the degradation process. In this work, the QS@PTh composite was synthesized, characterized, and used for the activation of PMS to degrade OG. To assess the ability of QS@PTh to activate PMS for Orange G degradation, the effect of several parameters was investigated including the catalyst dose, PMS dose, initial pH, initial OG concentration, and temperature of OG solution. Furthermore, the mechanism of PMS activation was suggested based on the results of quenching experiments and electron paramagnetic resonance (EPR) analysis.

# 2. Experimental

## 2.1. Preparation of the QS@PTh composite

The chemical reagents employed are presented in the ESI,† Text S1. The preparation of QS@PTh involved a chemical oxidative polymerization process of thiophene and QS in chloroform, utilizing anhydrous iron chloride ($FeCl_3$) as the oxidant. Initially, a dispersion of 1 g of QS in 20 mL of chloroform was agitated for 20 min. Subsequently, 0.5 mL of thiophene was introduced into the suspension, followed by ultrasonic vibration for 30 min. A solution of iron chloride in 30 mL of chloroform, with a molar ratio of $FeCl_3$ to thiophene set at 1 : 1, was prepared. The $FeCl_3$ solution was then added dropwise to the mixture and agitated at room temperature for 6 h. The addition of the oxidant ($FeCl_3$) resulted in a rapid color change to black, indicating the occurrence of oxidative polymerization. Afterward, the obtained solid product underwent filtration, followed by washing with distilled water and acetone, and was then dried at 60 °C overnight for subsequent use. To synthesize pure PTh, the same procedure was followed, excluding the addition of sand particles.

## 2.2. Characterization

The comprehensive characterization information is provided in the ESI,† Text S2.

## 2.3. Catalytic experiments

To evaluate the effectiveness of QS@PTh in activating PMS, batch experiments were conducted. The catalytic reaction took place in a 100 mL beaker, containing a specific amount of the catalyst, a certain quantity of peroxymonosulfate, and 50 mL of OG (50 mg $L^{-1}$), while being stirred for 60 min. Various factors were investigated, including PMS dosages (1–2.5 mM), catalyst dosages (0.1–0.4 g $L^{-1}$), initial pH values (ranging from 3.6 to 9.6), initial OG concentrations (ranging from 25 to 100 mg $L^{-1}$), and temperatures (ranging from 25 to 45 °C). The initial pH adjustment was performed with either NaOH (1 M) or HCl (1 M). Additionally, the performance of the QS@PTh/PMS system was assessed against that of other pollutants, including methyl orange (MO), rhodamine B (RhB), and bisphenol A (BPA), using the same experimental conditions as those of OG but varying the pollutant concentrations ([MO] = 50 mg $L^{-1}$, [RhB] = 20 mg $L^{-1}$, [BPA] = 10 mg $L^{-1}$). Following the degradation reaction, the remaining concentrations of the organic pollutants were determined using UV-vis spectroscopy at 464 nm, 554 nm, and 278 nm for MO, RhB, and BPA, respectively. The mineralization efficiency of OG in the QS@PTh/PMS system is typically measured using chemical oxygen demand (COD) by a colorimetric method based on standard methods for the examination of water and wastewater. To determine the reactive oxygen species (ROS) produced during PMS activation, quenching tests were carried out using various radical scavengers such as ethanol (EtOH), *tert*-butyl alcohol (TBA), *p*-benzoquinone (*p*-BQ), and L-histidine to trap $SO_4^{\bullet-}$, $^{\bullet}OH$, $O_2^{\bullet-}$, and $^1O_2$, respectively. To investigate the reusability and stability of QS@PTh, the used QS@PTh was centrifuged, washed with ethanol/distilled water, dried at 60 °C, and then reused under the same conditions.

# 3. Results and discussion

## 3.1. Characterization

Fig. 1(a) displays the X-ray diffraction patterns of two samples: QS and QS@PTh. In the case of QS, the X-ray diffraction pattern

Open Access Article. Published on 11 December 2023. Downloaded on 2/8/2026 11:39:59 PM.
This article is licensed under a Creative Commons Attribution-NonCommercial 3.0 Unported Licence.

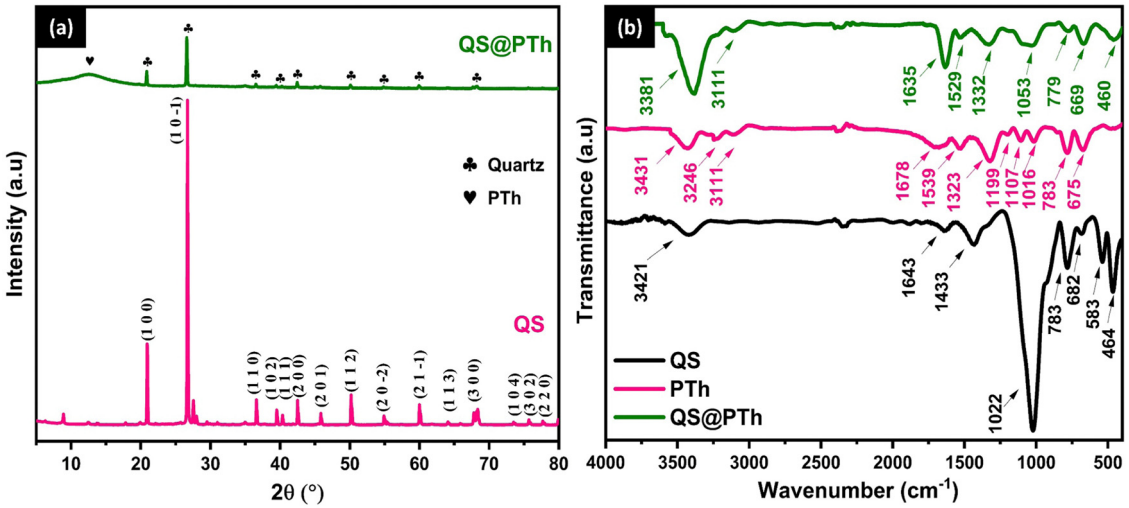


Fig. 1 The X-ray diffraction pattern of QS and QS@PTh (a), and the Fourier-transform infrared spectra of QS, PTh, and QS@PTh (b).

reveals distinct peaks at various angles, specifically 20.92°, 25.65°, 26.71°, 36.62°, 39.55°, 40.37°, 42.53°, 45.88°, 50.22°, 54.93°, 59.99°, 64.06°, 67.76°, 68.38°, 73.58°, 75.68°, and 77.78°. These peaks correspond to the crystallographic planes (1 0 0), (1 0 −1), (1 1 0), (1 0 2), (1 1 1), (2 0 0), (2 0 1), (1 1 2), (2 0 −2), (2 1 −1), (1 1 3), (3 0 0), (3 0 −1), (1 0 4), (3 0 2), and (2 2 0), respectively. These peaks align with the characteristic reflections of Quartz ($SiO_2$) as indicated by JCPDS card no 96-900-9667.[22] On the other hand, the XRD pattern of QS@PTh reveals the same peaks as those of QS, albeit with reduced intensities. Additionally, a new broad peak appears at 12.50°, which corresponds to the (001) plane, indicating an amorphous phase associated with the π–π stacking structure in polythiophene chains.[23] This observation confirms the successful formation of the QS@PTh composite.

The characteristic functional groups of QS, PTh, and QS@PTh, were analyzed by FTIR (Fig. 1(b)). The spectrum of QS exhibits distinct peaks at various wavenumbers. At 1022 $cm^{-1}$, a prominent peak is observed, while another peak is seen at 777 $cm^{-1}$. These peaks can be ascribed to the asymmetrical and symmetrical stretching vibrations of Si–O bonds, respectively.[24] Additionally, at 476 $cm^{-1}$ and 690 $cm^{-1}$, peaks can be observed, corresponding to the asymmetrical and symmetrical bending vibrations of Si–O bonds, respectively.[25] The peak at 541 $cm^{-1}$ is associated with the asymmetric bending vibration of Si–O–Al bonds.[26] Moreover, the peak detected at 1438 $cm^{-1}$ arises from the asymmetrical stretching vibration of $CO_3^{2-}$.[27] Lastly, the presence of a peak at 1633 $cm^{-1}$ and a broad band at 3425 $cm^{-1}$ indicates the bending and stretching vibrations, respectively, of O–H groups originating from water molecules adsorbed on the QS material.[28] In the case of polythiophene, the peak observed at 675 $cm^{-1}$ represents the C–S bending vibration.[29] The peak at 783 $cm^{-1}$ is assigned to the out of plane deformation mode of the C–H bond.[18] Moreover, the peaks at 1016 $cm^{-1}$, 1107 $cm^{-1}$, and 1199 $cm^{-1}$ correspond to the out of plane bending vibration of C–H.[30] The peak at 1323 $cm^{-1}$ is ascribed to the C–C stretching vibration of the thiophene ring,[31] while, the peaks at 1539 $cm^{-1}$ and 1678 $cm^{-1}$ belong to the symmetric and asymmetric stretching vibration of C=C bonds, respectively.[31] The peaks at 3111 $cm^{-1}$ and 3246 $cm^{-1}$ are assigned to the C–H asymmetric and symmetric stretching vibration in polythiophene, respectively.[19] The band at 3431 $cm^{-1}$ is associated with the O–H vibration of the adsorbed water. The QS@PTh composite showed the same characteristic peaks of PTh with a small shifting of the peaks to smaller wavenumbers, confirming that thiophene was successfully polymerized on QS.[18]

Fig. 2 presents surface morphology images of QS, PTh, and QS@PTh composite. Upon observing the figure, it becomes evident that QS (Fig. 2(a)) possesses a mostly rough surface with a few cracks on its outer layer. On the other hand, pure PTh (Fig. 2(b)) displays an irregular distribution and features a porous surface. In Fig. 2(c), the morphology of QS@PTh reveals the presence of prominently sized particles with a porous surface, providing confirmation that QS is successfully coated with PTh. The EDS-mapping analysis (Fig. 2(d)) displays the percentage and distribution of the main constituents of QS@PTh. The results reveal that eight elements (carbon, oxygen, aluminium, silicium, sulfur, chlorine, potassium, and iron) are evenly distributed on the surface of QS@PTh. These elements encompass significant components from both quartz sand (Si, O, Al, Cl, and Fe)[25] and PTh (C and S), confirming the successful preparation of the QS@PTh composite.

### 3.2. Catalytic performance of QS@PTh

**3.2.1. Degradation of OG in various systems.** Several experiments were carried out to assess the effectiveness of QS@PTh in removing OG from an aqueous solution. The results are presented in Fig. 3(a), showing both the removal efficiency and the corresponding rate constants. It is evident that PMS alone had minimal impact on degrading OG, with a constant rate of $8.9 \times 10^{-4}$ $min^{-1}$ after 60 min. This indicates that PMS alone is not efficient in degrading OG.[32] In contrast, when QS@PTh was used without PMS, only approximately


© 2024 The Author(s). Published by the Royal Society of Chemistry

Open Access Article. Published on 11 December 2023. Downloaded on 2/8/2026 11:39:59 PM.
This article is licensed under a Creative Commons Attribution-NonCommercial 3.0 Unported Licence.

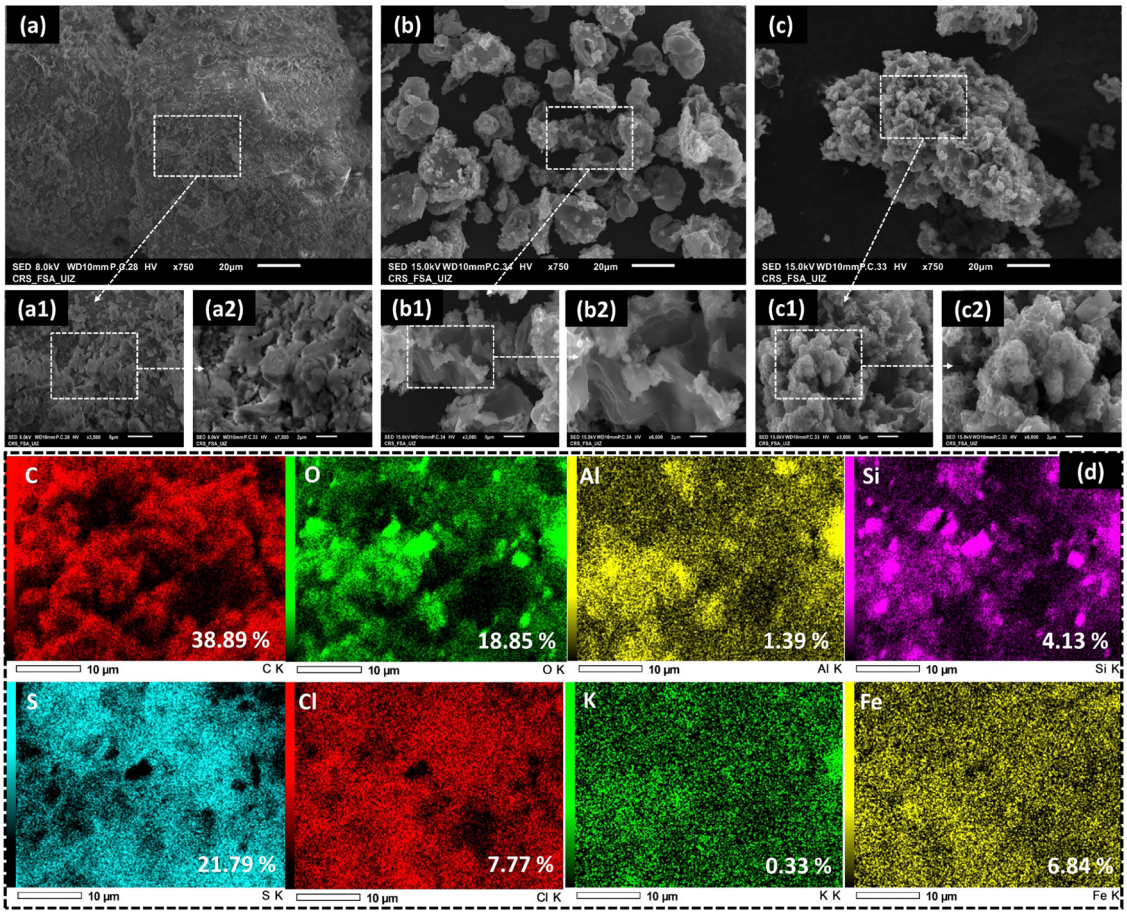


Fig. 2 SEM images of QS (a), PTh (b), and QS@PTh (c); the EDS elemental mapping of QS@PTh (d).

14.5% of OG was eliminated after 60 min, with a constant rate of 0.0028 $min^{-1}$, suggesting the negligible adsorption of OG onto QS@PTh. The degradation efficiencies of QS/PMS and PTh/PMS were approximately 15% and 23%, respectively. Remarkably, when QS@PTh/PMS was utilized, nearly 100% of OG was degraded within 60 min. Furthermore, the corresponding reaction rate constant was raised from 0.0028 $min^{-1}$ and 0.0046 $min^{-1}$ for QS/PMS and PTh/PMS, respectively, to 0.0711 $min^{-1}$ for QS@PTh/PMS. These findings provide confirmation that QS@PTh effectively activates PMS, leading to enhanced production of reactive oxygen species (ROS) for degrading OG molecules.

**3.2.2. Factors affecting degradation of OG by QS@PTh.** To assess the catalytic performance of QS@PTh/PMS in degrading OG, several factors including the PMS dose, catalyst dose, initial OG concentration, initial pH, and temperature were investigated. The results, depicted in Fig. 3, provide insight into these factors.

As displayed in Fig. 3(b), an increase in the PMS dose from 1 to 2.5 mM led to a corresponding increase in OG degradation efficiency from 43.82% to 100%, accompanied by an increase in $k_{app}$ from 0.0089 to 0.1304 $min^{-1}$. This could be ascribed to the generation of more reactive oxygen species (ROS) as the PMS dose increased,[33] thereby promoting the degradation efficiency. Nevertheless, it is worth noting that beyond a PMS dose of 1.5 mM, only a slight increase in $k_{app}$ was observed. Taking cost into consideration, 1.5 mM was determined to be the optimal PMS dose for subsequent experiments.

Referring to Fig. 3(c), as the catalyst dose increased from 0.1 to 0.4 g $L^{-1}$, the degradation rate of OG increased from 76.97% to 100%. Furthermore, the associated reaction rate constant also increased from 0.0215 to 0.2137 $min^{-1}$. These results can be attributed to the increased number of active sites resulting from the higher catalyst dose, thereby enhancing the degradation rate.[34,35] Nevertheless, when the catalyst dose was increased to 0.2 g $L^{-1}$, the removal rate of OG was not dramatically increased, revealing that 0.2 g $L^{-1}$ can be chosen as the optimal catalyst dose.

To examine the influence of initial solution pH values on OG degradation, a thorough investigation was conducted. As depicted in Fig. 3(d), it was observed that more than 97% of OG was degraded within 60 min in the QS@PTh/PMS system when the initial pH values ranged from 3.6 to 9.6. The corresponding rate constant, $k_{app}$, for OG degradation across different pH values fell between 0.0530 and 0.0967 $min^{-1}$. This indicates that the pH level has a minimal impact on the stability of QS@PTh, allowing the generated radicals to remain active under various pH conditions.[36] From Fig. S2 (ESI†), it can be

Open Access Article. Published on 11 December 2023. Downloaded on 2/8/2026 11:39:59 PM.
This article is licensed under a Creative Commons Attribution-NonCommercial 3.0 Unported Licence.

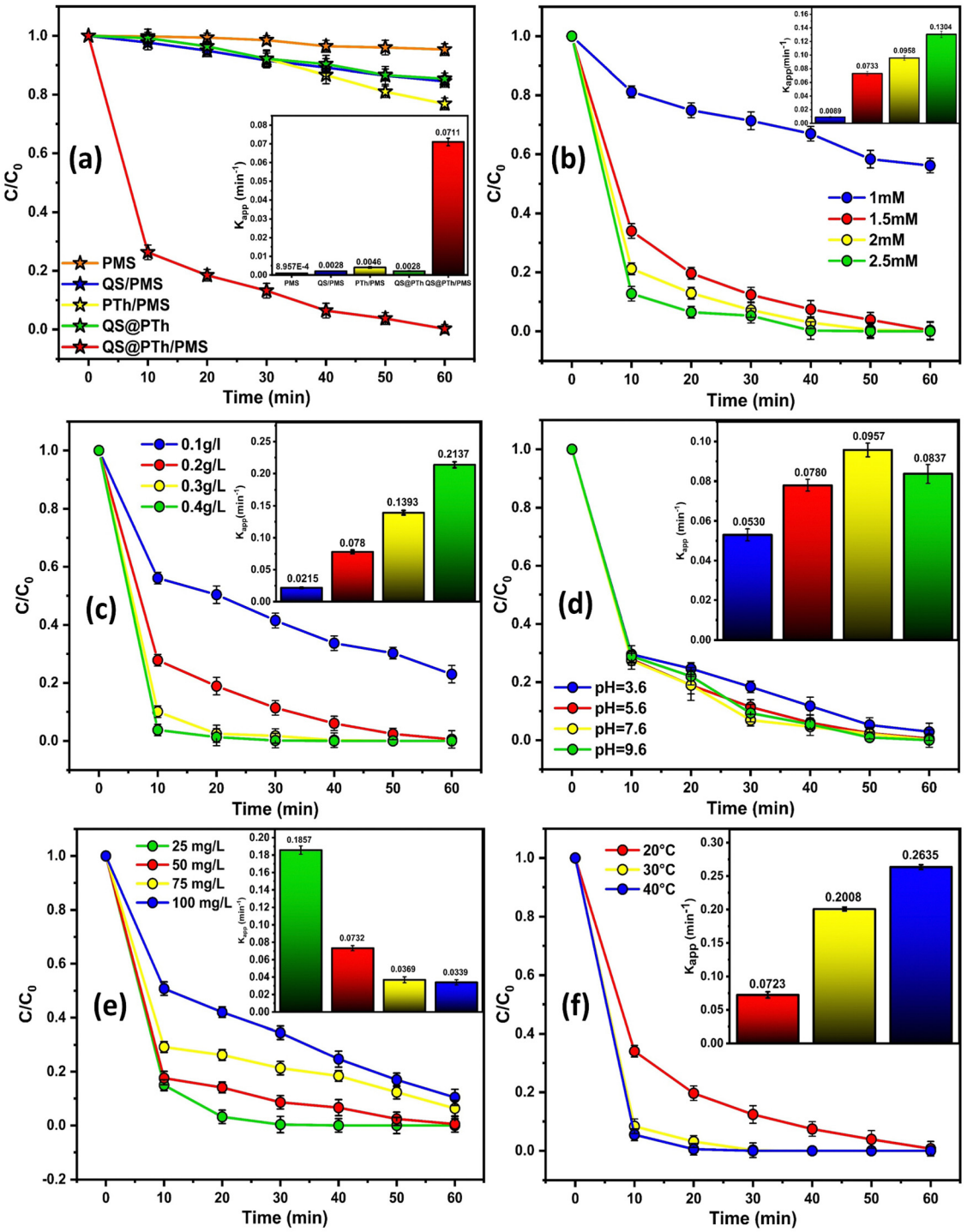


Fig. 3 Degradation of OG and the associated reaction rate constants in various systems (a); effects of various factors on OG degradation: PMS (b), QS@PTh dose (c), pH (d), OG concentration (e), and temperature (f).

seen that the $pH_{pzc}$ of QS@PTh is 8 which means that QS@PTh carries a positive charge when the pH is below 8 and a negative charge when the pH exceeds 8. Notably, the apparent rate constant ($k_{app}$) exhibits its highest values at approximately pH 7.6, which is in proximity to the point of zero charge. Conversely, under acidic and alkaline conditions, the $k_{app}$ values decrease. This phenomenon can be attributed to the $pK_a$ value of peroxymonosulfate ($pK_a$ = 9.4), signifying that $HSO_5^-$ prevails within the pH range of 3.6 to 7.6.[36] Under acidic conditions, the decrease in $k_{app}$ can be ascribed to interactions between $H^+$ ions and the more electronegative PMS, resulting in weaker repulsion at the interface between $HSO_5^-$ and the positively charged surface of QS@PTh.[37] This leads to a reduced efficiency in degrading Orange G dye. Under alkaline


© 2024 The Author(s). Published by the Royal Society of Chemistry

Open Access Article. Published on 11 December 2023. Downloaded on 2/8/2026 11:39:59 PM. This article is licensed under a Creative Commons Attribution-NonCommercial 3.0 Unported Licence.

conditions, the decrease in degradation efficiency is due to the self-decomposition of $HSO_5^-$ based on eqn (1).[38,39] In summary, these results highlight the exceptional pH adaptability of QS@PTh, demonstrating its effectiveness across a wide pH range.

$$2HSO_5^- + OH^- \rightarrow 2SO_4^{2-} + H_2O + O_2 \quad (1)$$

Based on Fig. 3(e), it is evident that an increase in the initial OG concentration from 25 to 100 mg $L^{-1}$ led to a decrease in the degradation efficiency from 100% to 89.56%. Similarly, their corresponding rate constant, $k_{app}$, dropped from 0.1857 to 0.0339 $min^{-1}$. This observation can be explained by two factors: first, the generation of degradation intermediates, which compete with the OG molecules,[40] and second, the occupation of available reactive sites on the QS@PTh surface, hindering the mass transfer from OG to QS@PTh.[41,42] However, even for an initial concentration of 100 mg $L^{-1}$, QS@PTh demonstrates high efficiency by removing 89% of Orange G, suggesting that QS@PTh is an efficient catalyst for PMS activation.

Generally, employing polymer-based catalysts can effectively activate PMS to degrade diverse organic pollutants such as pharmaceuticals, pesticides, and organic dyes. Table 1 compares the performance of the QS@PTh composite catalyst with other conducting polymer-based catalysts as activators for peroxymonosulfate (PMS) in the degradation of various organic contaminants. By comparing the degradation efficiencies achieved under different conditions, it becomes evident that the QS@PTh composite exhibits superior catalytic performance compared to other conducting polymer-based catalysts. It demonstrates higher degradation efficiencies, even at lower catalyst and oxidant concentrations, as well as at milder reaction temperatures and a broad pH range. These findings underscore the exceptional potential of the QS@PTh composite as a potential and versatile catalyst for PMS activation and degradation of diverse organic contaminants, offering promising prospects for application in environmental remediation.

From Fig. 3(f), it can be seen that an increase in temperature from 20 °C to 40 °C improved the degradation efficiency of OG, with a rate reaching 99.31% at 20 °C within 60 min and 100% at 40 °C within 30 min. Additionally, the associated rate constant rose from 0.0723 to 0.2635 $min^{-1}$. These findings suggest that higher temperatures facilitate the breaking of the O–O bond and the creation of $SO_4^{\bullet -}$.[47] To determine the activation energy ($E_a$), the Arrhenius equation (eqn (2)) was employed by plotting Ln ($k_{app}$) against $1/T$, as depicted in Fig. S2 (ESI†). The equation is defined as follows:

$$\mathrm{Ln}K_{app} = \mathrm{Ln}A - \frac{E_a}{RT} \quad (2)$$

Here, $A$ represents the pre-exponential parameter ($min^{-1}$), $E_a$ denotes the activation energy (KJ $mol^{-1}$), $R$ stands for the ideal gas reaction constant (8.314 kJ $mol^{-1}$ $K^{-1}$), and $T$ indicates the temperature ($K$). The activation energy ($E_a$) reflects the relative ease of pollutant degradation. For QS@PTh/PMS, the value of the activation energy is 51.24 kJ $mol^{-1}$, which exceeds the typical range of activation energy for diffusion–controlled reactions (10–13 kJ $mol^{-1}$). This suggests that the apparent reaction rate for this process is primarily influenced by the intrinsic chemical reactions occurring on the QS@PTh surface, rather than being influenced by the rate of mass transfer.[48]

Table 2 presents a comparison of the activation energy values for different catalysts in combination with the PMS system for OG degradation. Notably, the $E_a$ value for QS@PTh/PMS was considerably lower than that reported for other systems, indicating that the oxidation process facilitated by QS@PTh/PMS is more favorable and holds great promise for catalytic applications.

**3.2.3. Application for other organic pollutants and real water.** To assess the catalytic efficiency of QS@PTh in activating peroxymonosulfate (PMS) for the elimination of diverse organic contaminants, degradation experiments were conducted on various pollutants such as MO, RhB, and BPA. As illustrated in Fig. 4(a), the results reveal that the degradation rates for the majority of these pollutants exceeded 83% within a relatively short period of 60 min. This underscores the impressive capability of QS@PTh in expediting the breakdown of PMS, generating the active species crucial for oxidizing a broad spectrum of organic pollutants. Furthermore, the practical applicability of QS@PTh was evaluated under real conditions by examining its catalytic activity in tap water (TW) for the degradation of OG.

Table 1 The performances of conducting polymer-based catalysts as activators of PS/PMS for the degradation of different organic contaminants

| Pollutants | Catalysts | Pollutant concentration (mg $L^{-1}$) | Catalyst dose (g $L^{-1}$) | Oxidant dose (mM) | pH | Reaction time (min) | $T$ (°C) | Degradation efficiency (%) | Ref. |
|---|---|---|---|---|---|---|---|---|---|
| Orange G | QS@PTh | 50 | 0.2 | 1.5 (PMS) | 5.6 | 60 | 20 | 99.31 | This study |
| Orange G | N doped carbon (NC) | 50 | 0.2 | 4 (PS) | 5 | 24 | 25 | 80 | 9 |
| Orange G | S doped carbon (SC) | 50 | 0.2 | 4 (PS) | 5 | 24 | 25 | 100 | 9 |
| Orange G | N and S co-doped carbon (NSC) | 50 | 0.2 | 4 (PS) | 5 | 15 | 25 | 100 | 9 |
| Orange G | PANI@Alg | 50 | 0.2 | 4 (PS) | 5.2 | 30 | 25 | 100 | 43 |
| Orange G | PPY@Alg | 50 | 0.2 | 4 (PS) | 5.2 | 35 | 25 | 100 | 43 |
| Orange G | HS@PANI | 50 | 0.2 | 4 (PS) | 6.3 | 60 | 20 | 100 | 17 |
| Orange G | HS@PPY | 50 | 0.2 | 4 (PS) | 6.3 | 60 | 20 | 100 | 17 |
| Phenol | CPANI-9 | 941.1 | 0.025 | 0.5 (PMS) | 7 | 10 | 25 | 100 | 44 |
| Phenol | CPPy-F-8 | 20 | 0.1 | 3.25 (PMS) | 2.8 | 120 | 25 | 97 | 45 |
| Tetracycline | $Co_3O_4$/CPANI | 20 | 0.15 | 1.5 (PMS) | 5.5 | 40 | 25 | 92.11 | 33 |
| Tetracycline | $Fe_3O_4$@PANI-p | 20 | 0.4 | 4 (PMS) | 5 | 90 | 30 | 89.8 | 46 |

Open Access Article. Published on 11 December 2023. Downloaded on 2/8/2026 11:39:59 PM.
This article is licensed under a Creative Commons Attribution-NonCommercial 3.0 Unported Licence.

Table 2 Comparison of the activation energy values for different catalysts in combination with the PMS system for OG degradation

| Catalysts | Pollutants | Active agent | $E_a$ (KJ mol$^{-1}$) | Ref. |
|---|---|---|---|---|
| QS@PTh | Orange G | PMS | 51.24 | This study |
| $NH_2OH/Fe_3O_4$ | Orange G | PMS | 54.8 | 49 |
| Magnetic $MnFe_2O_4/\alpha$-$MnO_2$ | Orange G | PMS | 66.90 | 50 |
| $Fe^{2+}$ | Orange G | PMS | 92.2 | 51 |
| Carbon nanotubes | Orange G | PMS | 88.45 | 52 |

The findings shown in Fig. 4(b) indicate a degradation rate of 78.51% in 60 min. The lower degradation rate in tap water compared to that in distilled water can be attributed to the presence of several organic and inorganic compounds in the solution,[34] which are known to pose challenges and can restrict catalytic performance. Nevertheless, these overall results underscore the potential of QS@PTh as an effective catalyst for the oxidation of a wide range of organic pollutants. Future studies could explore optimization strategies to enhance its performance in complex aqueous matrices.

**3.2.4. Orange G mineralization by COD analysis.** To examine the mineralization efficiency of the Orange G dye during the QS@PTh/PMS/OG operation, the alteration in chemical oxygen demand (COD) concentration was monitored. Based on Fig. 4(c) and (d), it is evident that after a 60 min reaction period, a 79.4% COD removal efficiency is observed, accompanied by a 99.5% decolorization efficiency. Notably, the decrease in color was markedly higher compared to COD removal, consistent with previous research findings.[34,53] This disparity is ascribed to the greater difficulty in oxidizing intermediate products compared to their original compounds, resulting in a notably slower reaction rate during oxidation.[54] Additionally, it can be inferred that the QS@PTh/PMS catalyst exhibited considerable COD removal efficiency, reflecting its capability to activate PMS and generate an excess of radicals in the process.

### 3.3. Reusability of QS@PTh

To evaluate the suitability of QS@PTh for wastewater treatment, its reusability and stability were thoroughly examined.[55] A total of five consecutive tests were conducted under identical experimental conditions, including 1.5 mM of PMS, 0.2 g L$^{-1}$ of

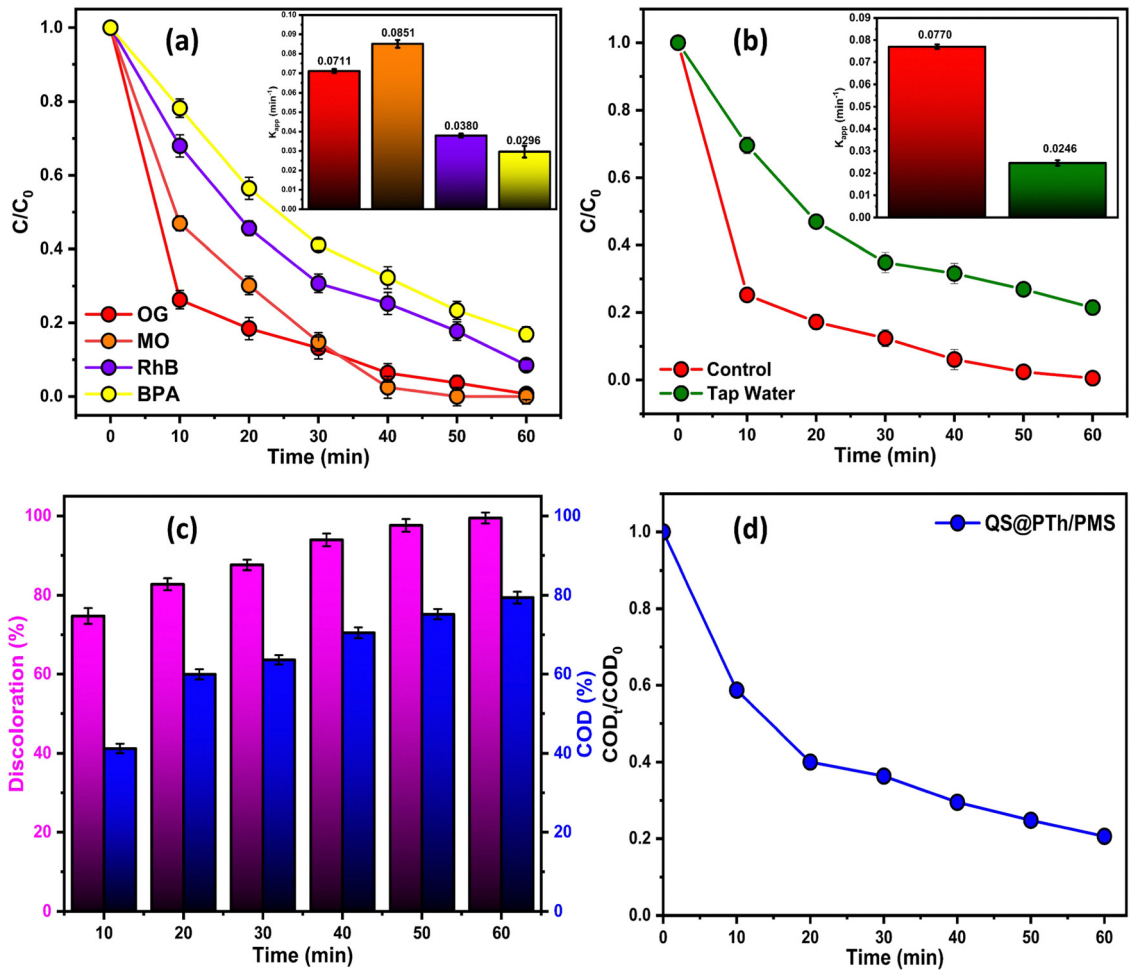


Fig. 4 Catalytic degradation of various organic pollutants in the QS@PTh/PMS system (a); OG degradation under real conditions (b); and OG mineralization by COD analysis (c) and (d).


© 2024 The Author(s). Published by the Royal Society of Chemistry

Open Access Article. Published on 11 December 2023. Downloaded on 2/8/2026 11:39:59 PM.
This article is licensed under a Creative Commons Attribution-NonCommercial 3.0 Unported Licence.

QS@PTh, $[OG]_0$ = 50 mg $L^{-1}$, initial pH of 6.0 (unadjusted), and a temperature of 20 °C. Following each cycle, the catalyst was collected, subjected to washing with distilled water and ethanol, and subsequently dried at 60 °C before reuse. The results displayed in Fig. 5(a) reveal that the degradation rate of OG utilizing the QS@PTh/PMS system decreased from 99.37% (1st run) to 97.48% (2nd run), 94.85% (3rd run), 91.54% (4th run), and 88.68% (5th run). The slight decrease in the OG degradation in the cyclic experiments of QS@PTh was probably due to the occupation of catalytic sites by the adsorbed OG and the reaction intermediates.[32,33,44] These outcomes confirmed that QS/PTh removes a significant amount of OG even after five recycles, making it a suitable catalyst for practical applications.

### 3.4. Reactive oxygen species (ROS) analysis and activation mechanisms

To obtain a more profound insight into the degradation process, quenching experiments were conducted to investigate the major reactive oxygen species generated in the QS@PTh/PMS system. For this purpose, specific agents were introduced into the reaction mixture: Ethanol was used to quench $^{\bullet}OH$ and $SO_4^{\bullet-}$ ($K_{\bullet OH/EtOH} = 10^9$ $M^{-1}$ $s^{-1}$, $K_{SO_4^{\bullet-}/EtOH} = 10^7$ $M^{-1}$ $s^{-1}$)[56]; TBA was employed to quench $^{\bullet}OH$ ($K_{\bullet OH/TBA} = 6.0 \times 10^8$ $M^{-1}$ $s^{-1}$).[57] The contribution of freely diffused $SO_4^{\bullet-}$ was concluded from the difference between the OG removal efficiency after adding EtOH and after adding TBA.[58] Additionally, P-BQ served as a scavenger of $O_2^{\bullet-}$ ($K_{O_2^{\bullet-}/P\text{-}BQ} = 9 \times 10^8$ $M^{-1}$ $s^{-1}$).[9] Moreover, L-histidine acted as a scavenger of $^1O_2$ ($k_{^1O_2/L\text{-}histidine} = 10^9$ $M^{-1}$ $s^{-1}$).[42] These additions were made to determine the primary species responsible for the degradation of Orange G in the QS@PTh/PMS system. The results presented in Fig. 5(b) demonstrate a degradation efficiency of 99.6% for the QS@PTh/PMS system, accompanied by a rate constant of 0.0776 $min^{-1}$. After the addition of EtOH and TBA to the system, the degradation rates decreased to 68.51% and 78.4%, respectively. Correspondingly, the rate constants ($k_{app}$) were reduced to 0.0175 $min^{-1}$ and 0.0209 $min^{-1}$, indicating the involvement of $^{\bullet}OH$ and $SO_4^{\bullet-}$ in the reaction process. These findings suggest that both $^{\bullet}OH$ and $SO_4^{\bullet-}$ played a role in the degradation of Orange G in the QS@PTh/PMS system. However, when P-BQ and was added to the system, the removal rate (99.65%) and the rate constant ($k_{app}$ = 0.0752 $min^{-1}$) remained almost constant, which means that the contribution of $O_2^{\bullet-}$ is excluded. It is important to note that benzoquinone can

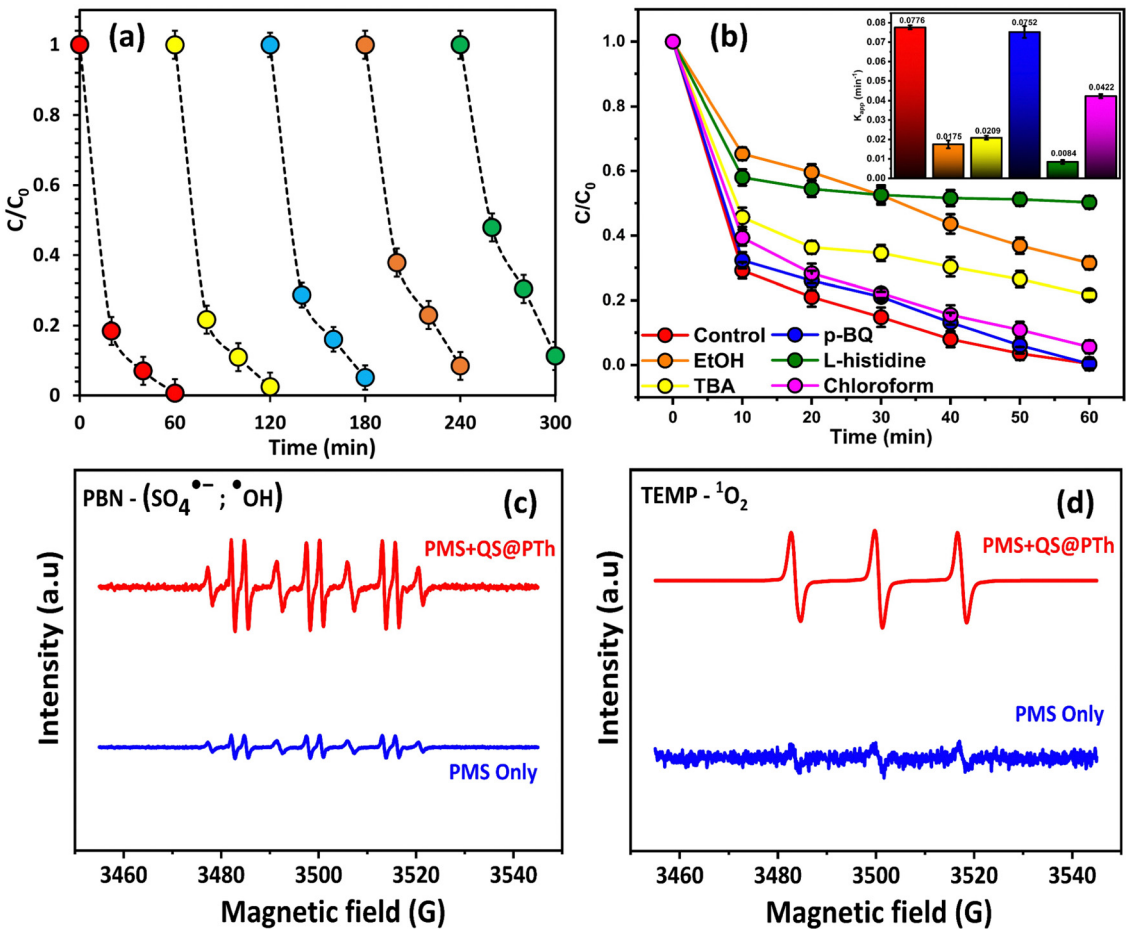


Fig. 5 Stability and reusability of QS@PTh (a), the effect of different radical scavengers on OG degradation and the corresponding reaction rate constants (b), EPR spectra with PBN (c) and TEMP (d) as the trapping agents.

Open Access Article. Published on 11 December 2023. Downloaded on 2/8/2026 11:39:59 PM. This article is licensed under a Creative Commons Attribution-NonCommercial 3.0 Unported Licence.

activate peroxymonosulfate to produce singlet oxygen, which can potentially influence the determination of the degradation mechanism.[59] Chloroform was also utilized as a scavenger for $O_2^{\bullet-}$ ($K_{O_2^{\bullet-}/\text{Chloroform}} = 10^{10}\ M^{-1}\ s^{-1}$) to confirm the contribution of superoxide ion radicals in the degradation process.[59,60] The results showed a removal rate of 94.4% and a rate constant of 0.0422 $min^{-1}$, suggesting a limited contribution of $O_2^{\bullet}$ in the degradation process. Furthermore, when L-histidine was introduced into the reaction system, the degradation efficiency and the rate constant were reduced to 49.71% and 0.0084 $min^{-1}$, respectively. Significantly, the ranking of inhibition in OG removal efficiency can be described as follows: L-histidine > EtOH > TBA > *p*-BQ, thereby confirming that $^1O_2$ served as the primary ROS in the degradation process, aligning with prior research findings.[61] Furthermore, the employment of PBN (phenyl-*tert*-butylnitrone) and TEMP (2,2,6,6-tetramethylpiperidine) in trapped electron paramagnetic resonance (EPR) tests serves to corroborate the principal reactive oxygen species (ROS).[9,43,62] PBN proves to be an effective scavenger, effectively inhibiting hydroxyl radicals ($^{\bullet}OH$) and sulfate radicals ($SO_4^{\bullet-}$), while TEMP serves as a scavenger for probing the signal of singlet oxygen ($^1O_2$).[63] As demonstrated in Fig. 5(c) and (d), when the catalysts are absent and only PMS is introduced into the reaction solutions, no distinctive signals are detected upon the addition of the spin-trapping agents (PBN, TEMP). However, with the introduction of QS@PTh into the system, characteristic EPR spectra emerge, depicting the adduct signals PBN-$SO_4^{\bullet-}$ and PBN-$^{\bullet}OH$. Additionally, as illustrated in the figure, the presence of the catalysts elicits a characteristic three-line signal, manifesting as a 1 : 1 : 1 triplet in the TEMP agent, attributable to the TEMP-$^1O_2$ adduct.[64] Consequently, these findings conclusively establish that the principal reactive species within the current systems encompass $SO_4^{\bullet-}$ and $^{\bullet}OH$ from the radical pathway, as well as $^1O_2$ originating from the non-radical pathway.

### 3.5. Catalytic mechanisms

As reported in the scientific literature, the key factor in activating PMS is the breaking of the superoxide O–O bond.[65] Thus, it became valuable to establish a pathway for electron flow between the catalyst's active sites and PMS. Building upon this theoretical framework and in light of the experimental data (see Fig. 5(b)–(d)), the activation pathways of PMS by QS@PTh were posited as a dual process involving both radical (minor) and non-radical (major) routes. The successful synthesis of QS@PTh was validated through comprehensive characterization studies. In this study, quartz sand was employed exclusively as a support material, suggesting that oxidation reactions primarily occurred between PTh and PMS. Polythiophene (PTh) possesses a conjugated system of alternating single and double bonds along its polymer backbone.[66] The sulfur atoms in polythiophene play a crucial role in activating PMS for the degradation of organic contaminants.[67] These sulfur atoms act as redox-active centers, facilitating electron transfer processes and initiating the generation of sulfate radicals ($SO_4^{\bullet-}$) and hydroxyl radicals ($^{\bullet}OH$) from PMS (eqn (3) and (4)). Consequently, the oxidation of organic substances can be attributed to the transfer of electrons from the quartz-sand@polythiophene composite (QS@PTh) to PMS. On the other hand, the $SO_4^{\bullet-}$, $^{\bullet}OH$, and QS@PTh-$S^{\bullet+}$ radical cations formed after electron transfer to PMS can react with $HSO_5^-$ molecules to produce the sulfate radical anion $SO_5^{\bullet-}$ (eqn (5)–(7)).[58,68] Moreover, the $SO_5^{\bullet-}$ formed in the system can react with $H_2O$ and $HSO_5^-$ to yield singlet oxygen $^1O_2$ (eqn (8) and (9)).[32,55] Overall, in the QS@PTh/PMS system, the degradation of OG was due to the combined effects of both radical species

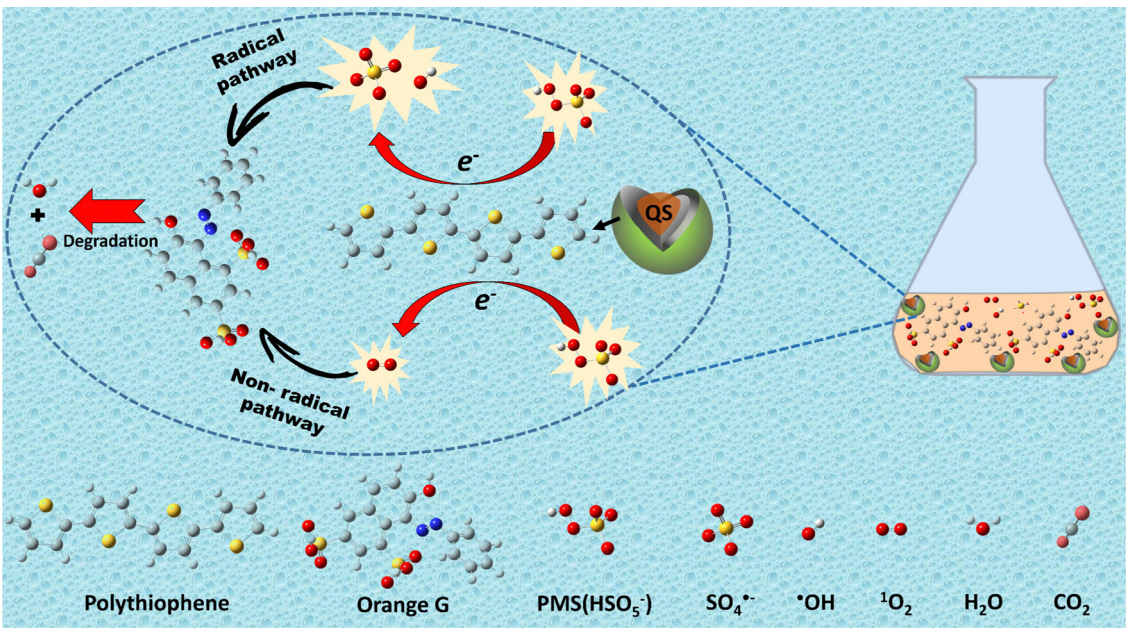


Fig. 6 The proposed mechanism of OG degradation in the QS@PTh/PMS system.


© 2024 The Author(s). Published by the Royal Society of Chemistry

Open Access Article. Published on 11 December 2023. Downloaded on 2/8/2026 11:39:59 PM. This article is licensed under a Creative Commons Attribution-NonCommercial 3.0 Unported Licence.

($^{\bullet}OH$ and $SO_4^{\bullet-}$) and non-radical species ($^1O_2$), where $^1O_2$ was the dominant active species. A portion of the OG was transformed into carbon dioxide ($CO_2$) and water ($H_2O$). The remaining fraction underwent degradation, and the resulting intermediates were adsorbed by the QS@PTh composite.[42]

$$\text{QS@PTh-S} + HSO_5^- \rightarrow \text{QS@PTh-S}^{\bullet+} + SO_4^{\bullet-} + OH^- \quad (3)$$

$$\text{QS@PTh-S} + HSO_5^- \rightarrow \text{QS@PTh-S}^{\bullet+} + SO_4^{2-} + {}^{\bullet}OH \quad (4)$$

$$\text{QS@PTh-S}^{\bullet+} + HSO_5^- \rightarrow \text{QS@PTh-S} + H^+ + SO_5^{\bullet-} \quad (5)$$

$$SO_4^{\bullet-} + HSO_5^- \rightarrow SO_5^{\bullet-} + H^+ + SO_4^{2-} \quad (6)$$

$${}^{\bullet}OH + HSO_5^- \rightarrow H_2O + SO_5^{\bullet-} \quad (7)$$

$$2SO_5^{\bullet-} + H_2O \rightarrow 2H^+ + 2SO_4^{2-} + 1.5\ {}^1O_2 \quad (8)$$

$$SO_5^{\bullet-} + HSO_5^- \rightarrow HSO_4^- + SO_4^{2-} + {}^1O_2 \quad (9)$$

$$\text{ROSs} + \text{OG} \rightarrow \text{Intermediates} + CO_2 + H_2O \quad (10)$$

In light of the aforementioned findings, a mechanism illustrating the activation of PMS by QS@PTh for the OG degradation was proposed, as depicted in Fig. 6.

## Conclusions

This study explores the use of a quartz-sand@polythiophene composite as a highly efficient catalyst for activating PMS in the degradation of the Orange G dye. The composite material was synthesized using a facile and cost-effective method, combining the unique properties of both quartz sand and polythiophene. The effects of various factors, such as PMS concentration, catalyst dosage, pH, initial concentration of OG, and temperature, were systematically investigated. The results revealed that the QS@PTh/PMS composite exhibited excellent catalytic activity, achieving a 99.5% degradation efficiency of OG (50 mg $L^{-1}$) and an 79.4% reduction in COD within 60 min, under specific optimized conditions: 1.5 mM PMS concentration, 0.2 g $L^{-1}$ of QS@PTh, a pH of 5.6, and a temperature of 20 °C. Furthermore, the results indicated that QS@PTh/PMS displayed high catalytic activity over a broad pH range and outperformed other catalysts with an activation energy of 51.24 kJ $mol^{-1}$ for OG degradation. On the other hand, QS@PTh/PMS has shown very good performance in the degradation (>83%) of different pollutants (MO, RhB, and PBA). Additionally, the degradation experiments in real water showed a degradation rate of 78.51% in 60 min. Furthermore, the catalyst exhibited outstanding stability and reusability, maintaining its catalytic activity even after five consecutive cycles. The degradation mechanism was investigated through the examination of reactive species using quenching experiments and EPR analysis. The results demonstrated the involvement of $SO_4^{\bullet-}$, $^{\bullet}OH$, and $^1O_2$ in the degradation of OG by the QS@PTh/PMS system. Overall, this study highlights the significant potential of the QS@PTh composite as an effective catalyst for Orange G degradation using PMS as an oxidizing agent. The findings contribute to the advancement of environmentally friendly and sustainable solutions for the remediation of wastewater, opening new avenues for the application of composite catalysts in advanced oxidation processes.

## Conflicts of interest

The authors declare that they have no known competing financial interests or personal relationships that could have appeared to influence the work reported in this paper.

## References

1 R. Al-Tohamy, S. S. Ali, F. Li, K. M. Okasha, Y. A. G. Mahmoud, T. Elsamahy, H. Jiao, Y. Fu and J. Sun, A critical review on the treatment of dye-containing wastewater: Ecotoxicological and health concerns of textile dyes and possible remediation approaches for environmental safety, *Ecotoxicol. Environ. Saf.*, 2022, **231**, 113160, DOI: **10.1016/J.ECOENV.2021.113160**.

2 S. Farsad, A. Amjlef, A. Chaoui, A. Ben Hamou, C. Hamma, M. Benafqir, A. Jada and N. El Alem, Harnessing a carbon-based material from food waste digestate for dye adsorption: the role of hydrogel beads in enhancing the material stability and regenerative capacity, *Mater. Adv.*, 2023, **4**(24), 6599–6611, DOI: **10.1039/D3MA00505D**.

3 B.-E. Channab, M. El Ouardi, O. Ait Layachi, S. E. Marrane, A. El Idrissi, A. BaQais and H. Ait Ahsaine, Recent trends on MIL-Fe metal–organic frameworks: synthesis approaches, structural insights, and applications in organic pollutant adsorption and photocatalytic degradation, *Environ. Sci.: Nano*, 2023, **10**, 2957–2988, DOI: **10.1039/D3EN00332A**.

4 S. Farsad, A. Ben Hamou, A. Chaoui, A. Amjlef, S. Lhanafi, S. Et-Taleb and N. El Alem, Maximizing bio-methane potential from municipal landfill leachate through ultrasonic pretreatment, *Heliyon*, 2023, **9**, e21347, DOI: **10.1016/j.heliyon.2023.e21347**.

5 S. Farsad, Z. Anfar, A. Ait El Fakir, A. Amjlef, N. El Alem and I. Ionel, Methane recovery from the leachate of municipal solid waste landfill by using anaerobic digestion. case study, in *European Biomass Conference and Exhibition*, 2022, pp. 223–227.

6 R. Pelalak, A. Hassani, Z. Heidari and M. Zhou, State-of-the-art recent applications of layered double hydroxides (LDHs) material in Fenton-based oxidation processes for water and wastewater treatment, *Chem. Eng. J.*, 2023, **474**, 145511, DOI: **10.1016/j.cej.2023.145511**.

7 S. Wu, W. Wu, J. Fan, L. Zhang, Y. Zhong, H. Xu and Z. Mao, Rapid activation of peroxymonosulfate with iron(III) complex for organic pollutants degradation *via* a non-radical pathway, *Water Res.*, 2023, **233**, 119725, DOI: **10.1016/J.WATRES.2023.119725**.

8 Y. Wang, Y. Tong, D. Chen, T. Zhou, Q. Zhang and J. P. Zou, Activation of peroxymonosulfate by g-$C_3N_4$/ε-$MnO_2$ microspheres for nonradical pathway degradation of organic pollutants in water: Catalytic mechanism and degradation

Open Access Article. Published on 11 December 2023. Downloaded on 2/8/2026 11:39:59 PM. This article is licensed under a Creative Commons Attribution-NonCommercial 3.0 Unported Licence.

path, *Chem. Eng. J.*, 2023, **459**, 141643, DOI: 10.1016/J.CEJ.2023.141643.

9 A. Ait El Fakir, Z. Anfar, M. Enneiymy, A. Jada and N. El Alem, Conjugated polymers templated carbonization to design N, S co-doped finely tunable carbon for enhanced synergistic catalysis, *Appl. Catal., B*, 2022, **300**, 120732, DOI: 10.1016/J.APCATB.2021.120732.

10 Z. Sun, X. Liu, X. Dong, X. Zhang, Y. Tan, F. Yuan, S. Zheng and C. Li, Synergistic activation of peroxymonosulfate via in situ growth $FeCo_2O_4$ nanoparticles on natural rectorite: Role of transition metal ions and hydroxyl groups, *Chemosphere*, 2021, **263**, 127965, DOI: 10.1016/J.CHEMOSPHERE.2020.127965.

11 J. Wang and S. Wang, Activation of persulfate (PS) and peroxymonosulfate (PMS) and application for the degradation of emerging contaminants, *Chem. Eng. J.*, 2018, **334**, 1502–1517, DOI: 10.1016/J.CEJ.2017.11.059.

12 S. Liu, Z. Zhang, F. Huang, Y. Liu, L. Feng, J. Jiang, L. Zhang, F. Qi and C. Liu, Carbonized polyaniline activated peroxymonosulfate (PMS) for phenol degradation: Role of PMS adsorption and singlet oxygen generation, *Appl. Catal., B*, 2021, **286**, 119921, DOI: 10.1016/j.apcatb.2021.119921.

13 S. Saini, K. Kumar, P. Saini, D. K. Mahawar, K. S. Rathore, S. Kumar, A. Dandia and V. Parewa, Sustainable synthesis of biomass-derived carbon quantum dots and their catalytic application for the assessment of α,β-unsaturated compounds, *RSC Adv.*, 2022, **12**, 32619–32629, DOI: 10.1039/D2RA05201F.

14 C. Wang, Y. Liu, F. Han, Y. Han, T. Liu, H. Ren and X. Han, Nitrogen-doped carbocatalyst activated persulfate (PS) for oxidation polymerization of bisphenol A (BPA): importance of nonradical activation of PS, *Phys. Chem. Chem. Phys.*, 2023, **25**, 13716–13727, DOI: 10.1039/D3CP00659J.

15 S. Annamalai and W. S. Shin, In-situ pyrolysis of Undaria pinnatifida as a green carbo-catalyst for degradation of organic contaminants: Role of inherent N and P in the degradation pathway, *Chem. Eng. J.*, 2023, **465**, 142813, DOI: 10.1016/J.CEJ.2023.142813.

16 M. Cheng, Y. Zhang, B. Lai, L. Wang, S. Yang, K. Li, D. Wang, Y. Wu, G. H. Chen and J. Qian, Nitrogen and phosphorus co-doped porous carbons (NPCs) for peroxydisulfate (PDS) activation towards tetracycline degradation: Defects enhanced adsorption and non-radical mechanism dominated by electron transfer, *Chem. Eng. J.*, 2023, **455**, 140615, DOI: 10.1016/J.CEJ.2022.140615.

17 A. Ait El Fakir, Z. Anfar, A. Amedlous, A. Amjlef, S. Farsad, A. Jada and N. El Alem, Synergistic effect for efficient catalytic persulfate activation in conducting polymers-hematite sand composites: Enhancement of chemical stability, *Appl. Catal., A*, 2021, **623**, 118246, DOI: 10.1016/J.APCATA.2021.118246.

18 A. Husain, S. Ahmad and F. Mohammad, Electrical conductivity and ammonia sensing studies on polythiophene/MWCNTs nanocomposites, *Materialia*, 2020, **14**, 100868, DOI: 10.1016/J.MTLA.2020.100868.

19 A. Husain, S. Ahmad, M. U. Shariq and M. M. A. Khan, Ultrasensitive, highly selective and completely reversible ammonia sensor based on polythiophene/SWCNT nanocomposite, *Materialia*, 2020, **10**, 100704, DOI: 10.1016/J.MTLA.2020.100704.

20 S. S. Bulla, R. F. Bhajantri, C. Chavan and K. Sakthipandi, Synthesis and characterization of polythiophene/zinc oxide nanocomposites for chemiresistor organic vapor-sensing application, *J. Polym. Res.*, 2021, **28**, 251, DOI: 10.1007/s10965-021-02618-7.

21 X. Z. Guo, Y. F. Kang, T. L. Yang and S. R. Wang, Low-temperature $NO_2$ sensors based on polythiophene/WO3 organic-inorganic hybrids, *Trans. Nonferrous Met. Soc. China*, 2012, **22**, 380–385, DOI: 10.1016/S1003-6326(11)61187-4.

22 M. Hernández-Chávez, M. Vargas-Ramírez, A. M. Herrera-González, J. García-Serrano, M. Hernández-Chávez, A. C. Ramírez, R. G. Romero-Serrano and J. A. Sánchez-Alvarado, Thermodynamic analysis of the influence of potassium on the thermal behavior of kaolin raw material, *Physicochem. Probl. Miner. Process.*, 2020, **57**, 39–52, DOI: 10.37190/PPMP/128393.

23 R. Singh, A. K. Bajpai and A. K. Shrivastava, CdSe nanorod-reinforced poly(thiophene) composites in designing energy storage devices: study of morphology and dielectric behavior, *Polym. Bull.*, 2021, **78**, 115–131, DOI: 10.1007/S00289-020-03104-8/METRICS.

24 A. Amjlef, S. Farsad, A. Ait El Fakir, A. El Asri, S. El Issami, S. Et-Taleb and N. El Alem, Polyaniline-encapsulated quartz sand as an adsorbent composite for Orange G dye removal from aqueous solution: Experimental and computational study, *Ceram. Int.*, 2023, **49**(9), 14120–14134, DOI: 10.1016/J.CERAMINT.2022.12.293.

25 A. Amjlef, S. Khrach, A. Ait El Fakir, S. Farsad, S. Et-Taleb and N. El Alem, Adsorptive properties investigation of natural sand as adsorbent for methylene blue removal from contaminated water, *Nanotechnol. Environ. Eng.*, 2021, **6**, 26, DOI: 10.1007/s41204-021-00119-y.

26 R. El Haouti, Z. Anfar, S. Et-Taleb, M. Benafqir, S. Lhanafi and N. El Alem, Removal of heavy metals and organic pollutants by a sand rich in iron oxide, *Eur. Mediterr. J. Environ. Integr.*, 2018, **3**(1), 17, DOI: 10.1007/s41207-018-0058-9.

27 N. Meftah and M. S. Mahboub, Spectroscopic Characterizations of Sand Dunes Minerals of El-Oued (Northeast Algerian Sahara) by FTIR, XRF and XRD Analyses, *Silicon*, 2020, **12**, 147–153, DOI: 10.1007/s12633-019-00109-5.

28 A. Amjlef, S. Farsad, A. Chaoui, A. Ben Hamou, M. Ezzahery, S. Et-Taleb and N. El Alem, Effective adsorption of Orange G dye using chitosan cross-linked by glutaraldehyde and reinforced with quartz sand, *Int. J. Biol. Macromol.*, 2023, 124373, DOI: 10.1016/J.IJBIOMAC.2023.124373.

29 C.-S. Park, D. Y. Kim, E. Y. Jung, H. J. Jang, G. T. Bae, J. Y. Kim, B. J. Shin, H.-K. Lee and H.-S. Tae, Ultrafast Room Temperature Synthesis of Porous Polythiophene via Atmospheric Pressure Plasma Polymerization Technique and Its Application to $NO_2$ Gas Sensors, *Polymers*, 2021, **13**(11), 1783, DOI: 10.3390/polym13111783.

30 A. Husain, S. Ahmad and F. Mohammad, Synthesis, characterisation and ethanol sensing application of polythiophene/

 © 2024 The Author(s). Published by the Royal Society of Chemistry

Open Access Article. Published on 11 December 2023. Downloaded on 2/8/2026 11:39:59 PM. This article is licensed under a Creative Commons Attribution-NonCommercial 3.0 Unported Licence.

graphene nanocomposite, *Mater. Chem. Phys.*, 2020, **239**, 122324, DOI: 10.1016/J.MATCHEMPHYS.2019.122324.

31 A. Husain, S. Ahmad, S. P. Ansari, M. O. Ansari and M. M. A. khan, DC electrical conductivity retention and acetone/acetaldehyde sensing on polythiophene/molybdenum disulphide composites, *Polym. Polym. Compos.*, 2021, **29**, S422–S431, DOI: 10.1177/09673911211002781.

32 C. Huang, Y. Wang, M. Gong, W. Wang, Y. Mu and Z. H. Hu, A-MnO2/Palygorskite composite as an effective catalyst for heterogeneous activation of peroxymonosulfate (PMS) for the degradation of Rhodamine B, *Sep. Purif. Technol.*, 2020, **230**, 115877, DOI: 10.1016/j.seppur.2019.115877.

33 J. Qian, X. Mi, Z. Chen, W. Xu, W. Liu, R. Ma, Y. Zhang, Y. Du and B. J. Ni, Efficient emerging contaminants (EM) decomposition via peroxymonosulfate (PMS) activation by Co3O4/carbonized polyaniline (CPANI) composite: Characterization of tetracycline (TC) degradation property and application for the remediation of EM-polluted wate, *J. Cleaner Prod.*, 2023, **405**, 137023, DOI: 10.1016/j.jclepro.2023.137023.

34 S. Madihi-Bidgoli, S. Asadnezhad, A. Yaghoot-Nezhad and A. Hassani, Azurobine degradation using $Fe_2O_3$@multi-walled carbon nanotube activated peroxymonosulfate (PMS) under UVA-LED irradiation: performance, mechanism and environmental application, *J. Environ. Chem. Eng.*, 2021, **9**, 106660, DOI: 10.1016/j.jece.2021.106660.

35 P. K. Klu, M. A. Nasir Khan, C. Wang, J. Qi, X. Sun and J. Li, Mechanism of peroxymonosulfate activation and the utilization efficiency using hollow $(Co, Mn)_3O_4$ nanoreactor as an efficient catalyst for degradation of organic pollutants, *Environ. Res.*, 2022, **207**, 112148, DOI: 10.1016/J.ENVRES.2021.112148.

36 R. Bai, Y. Xiao, W. Yan, S. Wang, R. Ding, F. Yang, J. Li, X. Lu and F. Zhao, Rapid and efficient removal of naproxen from water by CuFe2O4 with peroxymonosulfate, *Environ. Sci. Pollut. Res.*, 2020, **27**, 21542–21551, DOI: 10.1007/s11356-020-08613-7.

37 G. Wang, S. Chen, X. Quan, H. Yu and Y. Zhang, Enhanced activation of peroxymonosulfate by nitrogen doped porous carbon for effective removal of organic pollutants, *Carbon*, 2017, **115**, 730–739, DOI: 10.1016/J.CARBON.2017.01.060.

38 A. Hassani, P. Eghbali, F. Mahdipour, S. Wacławek, K. Y. A. Lin and F. Ghanbari, Insights into the synergistic role of photocatalytic activation of peroxymonosulfate by UVA-LED irradiation over $CoFe_2O_4$-rGO nanocomposite towards effective Bisphenol A degradation: Performance, mineralization, and activation mechanism, *Chem. Eng. J.*, 2023, **453**, 139556, DOI: 10.1016/J.CEJ.2022.139556.

39 Z. Wang, Y. Du, Y. Liu, B. Zou, J. Xiao and J. Ma, Degradation of organic pollutants by NiFe2O4/peroxymonosulfate: efficiency, influential factors and catalytic mechanism, *RSC Adv.*, 2016, **6**, 11040–11048, DOI: 10.1039/C5RA21117D.

40 Y. Song, L. Huang, X. Zhang, H. Zhang, L. Wang, H. Zhang and Y. Liu, Synergistic effect of persulfate and g-$C_3N_4$ under simulated solar light irradiation: Implication for the degradation of sulfamethoxazole, *J. Hazard. Mater.*, 2020, **393**, 122379, DOI: 10.1016/J.JHAZMAT.2020.122379.

41 J. Li, K. Zhu, R. Li, X. Fan, H. Lin and H. Zhang, The removal of azo dye from aqueous solution by oxidation with peroxydisulfate in the presence of granular activated carbon: Performance, mechanism and reusability, *Chemosphere*, 2020, **259**, 127400, DOI: 10.1016/J.CHEMOSPHERE.2020.127400.

42 P. Zhai, H. Liu, F. Sun, T. Chen, X. Zou, H. Wang, Z. Chu, C. Wang, M. Liu and D. Chen, Carbonization of methylene blue adsorbed on palygorskite for activating peroxydisulfate to degrade bisphenol A: An electron transfer mechanism, *Appl. Clay Sci.*, 2022, **216**, 106327, DOI: 10.1016/j.clay.2021.106327.

43 A. Ait El Fakir, Z. Anfar, A. Amedlous, M. Zbair, Z. Hafidi, M. El Achouri, A. Jada and N. El Alem, Engineering of new hydrogel beads based conducting polymers: Metal-free catalysis for highly organic pollutants degradation, *Appl. Catal., B*, 2021, **286**, 119948, DOI: 10.1016/j.apcatb.2021.119948.

44 S. Liu, Z. Zhang, F. Huang, Y. Liu, L. Feng, J. Jiang, L. Zhang, F. Qi and C. Liu, Carbonized polyaniline activated peroxymonosulfate (PMS) for phenol degradation: Role of PMS adsorption and singlet oxygen generation, *Appl. Catal., B*, 2021, **286**, 119921, DOI: 10.1016/J.APCATB.2021.119921.

45 P. Hu, H. Su, Z. Chen, C. Yu, Q. Li, B. Zhou, P. J. J. Alvarez and M. Long, Selective Degradation of Organic Pollutants Using an Efficient Metal-Free Catalyst Derived from Carbonized Polypyrrole via Peroxymonosulfate Activation, *Environ. Sci. Technol.*, 2017, **51**, 11288–11296, DOI: 10.1021/ACS.EST.7B03014/SUPPL_FILE/ES7B03014_SI_001.PDF.

46 Y. Q. Wang, K. Li, M. Y. Shang, Y. Z. Zhang, Y. Zhang, B. L. Li, Y. J. Kan, X. Q. Cao and J. Zhang, A novel partially carbonized $Fe_3O_4$@PANI-p catalyst for tetracycline degradation via peroxymonosulfate activation, *Chem. Eng. J.*, 2023, **451**, 138655, DOI: 10.1016/j.cej.2022.138655.

47 J. Deng, C. Ya, Y. Ge, Y. Cheng, Y. Chen, M. Xu and H. Wang, Activation of peroxymonosulfate by metal (Fe, Mn, Cu and Ni) doping ordered mesoporous $Co_3O_4$ for the degradation of enrofloxacin, *RSC Adv.*, 2018, **8**, 2338–2349, DOI: 10.1039/C7RA07841B.

48 L. Xu and J. Wang, Magnetic nanoscaled $Fe_3O_4/CeO_2$ composite as an efficient Fenton-like heterogeneous catalyst for degradation of 4-chlorophenol, *Environ. Sci. Technol.*, 2012, **46**, 10145–10153, DOI: 10.1021/ES300303F.

49 J. Zhang, M. Chen and L. Zhu, Activation of peroxymonosulfate by iron-based catalysts for orange G degradation: role of hydroxylamine, *RSC Adv.*, 2016, **6**, 47562–47569, DOI: 10.1039/C6RA07231C.

50 L. T. Thao, T. Van Nguyen, V. Q. Nguyen, N. M. Phan, K. J. Kim, N. N. Huy and N. T. Dung, Orange G degradation by heterogeneous peroxymonosulfate activation based on magnetic $MnFe_2O_4/\alpha$-$MnO_2$ hybrid, *J. Environ. Sci.*, 2023, **124**, 379–396, DOI: 10.1016/J.JES.2021.10.008.

51 X. R. Xu and X. Z. Li, Degradation of azo dye Orange G in aqueous solutions by persulfate with ferrous ion, *Sep. Purif. Technol.*, 2010, **72**, 105–111, DOI: 10.1016/J.SEPPUR.2010.01.012.

52 N. Nagar and V. Devra, Oxidative degradation of Orange G by peroxomonosulfate in presence of biosynthesized copper nanoparticles—A kinetic study, *Environ. Technol. Innov.*, 2018, **10**, 281–289, DOI: 10.1016/J.ETI.2018.03.005.

Open Access Article. Published on 11 December 2023. Downloaded on 2/8/2026 11:39:59 PM. This article is licensed under a Creative Commons Attribution-NonCommercial 3.0 Unported Licence.

53 B.-E. Channab, M. El Ouardi, S. E. Marrane, O. A. Layachi, A. El Idrissi, S. Farsad, D. Mazkad, A. BaQais, M. Lasri and H. Ait Ahsaine, Alginate@$ZnCO_2O_4$ for efficient peroxymonosulfate activation towards effective rhodamine B degradation: optimization using response surface methodology, *RSC Adv.*, 2023, **13**, 20150–20163, DOI: 10.1039/D3RA02865H.

54 C. Cai, H. Zhang, X. Zhong and L. Hou, Electrochemical enhanced heterogeneous activation of peroxydisulfate by Fe–Co/SBA-15 catalyst for the degradation of Orange II in water, *Water Res.*, 2014, **66**, 473–485, DOI: 10.1016/J.WATRES.2014.08.039.

55 Y. Zhang, Q. Peng, W. Zhong, J. Xing and K. Liu, Novel MnCo2O4.5@manganese sand for efficient degradation of tetracycline through activating peroxymonosulfate: Facile synthesis, adaptable performance and long-term effectiveness, *Colloids Surf., A*, 2023, **661**, 130915, DOI: 10.1016/J.COLSURFA.2022.130915.

56 R. Huang, P. Gao, J. Zhu, Y. Zhang, Y. Chen, S. Huang, G. Wang, Z. Yu, S. Zhao and S. Zhou, Insights into the pollutant electron property inducing the transformation of peroxymonosulfate activation mechanisms on manganese dioxide, *Appl. Catal., B*, 2022, **317**, 121753, DOI: 10.1016/j.apcatb.2022.121753.

57 J. Yao, Y. Yu, R. Qu, J. Chen, Z. Huo, F. Zhu and Z. Wang, Fe-Activated Peroxymonosulfate Enhances the Degradation of Dibutyl Phthalate on Ground Quartz Sand, *Environ. Sci. Technol.*, 2020, **54**, 9052–9061, DOI: 10.1021/acs.est.0c00793.

58 J. Zhou, X. Li, J. Yuan and Z. Wang, Efficient degradation and toxicity reduction of tetracycline by recyclable ferroferric oxide doped powdered activated charcoal via peroxymonosulfate (PMS) activation, *Chem. Eng. J.*, 2022, **441**, 136061, DOI: 10.1016/j.cej.2022.136061.

59 J. Wang and S. Wang, Reactive species in advanced oxidation processes: Formation, identification and reaction mechanism, *Chem. Eng. J.*, 2020, **401**, 126158, DOI: 10.1016/J.CEJ.2020.126158.

60 A. L. Teel and R. J. Watts, Degradation of carbon tetrachloride by modified Fenton's reagent, *J. Hazard. Mater.*, 2002, **94**, 179–189, DOI: 10.1016/S0304-3894(02)00068-7.

61 A. Hassani, J. Scaria, F. Ghanbari and P. V. Nidheesh, Sulfate radicals-based advanced oxidation processes for the degradation of pharmaceuticals and personal care products: A review on relevant activation mechanisms, performance, and perspectives, *Environ. Res.*, 2023, **217**, 114789, DOI: 10.1016/J.ENVRES.2022.114789.

62 A. Ait El Fakir, Z. Anfar, M. Enneiymy, A. Jada and N. El Alem, New insights into N, S doped carbon from conjugated polymers for efficient persulfate activation: Role of hydrogel beads in enhancement of stability, *Chem. Eng. J.*, 2022, **442**, 136055, DOI: 10.1016/j.cej.2022.136055.

63 X. Li, J. Wang, X. Duan, Y. Li, X. Fan, G. Zhang, F. Zhang and W. Peng, Fine-Tuning Radical/Nonradical Pathways on Graphene by Porous Engineering and Doping Strategies, *ACS Catal.*, 2021, **11**, 4848–4861, DOI: 10.1021/acscatal.0c05089.

64 X. Chen, J. Zhou, H. Yang, H. Wang, H. Li, S. Wu and W. Yang, PMS activation by magnetic cobalt-N-doped carbon composite for ultra-efficient degradation of refractory organic pollutant: Mechanisms and identification of intermediates, *Chemosphere*, 2022, **287**, 132074, DOI: 10.1016/j.chemosphere.2021.132074.

65 C. Yu, J. He, S. Lan, W. Guo and M. Zhu, Enhanced utilization efficiency of peroxymonosulfate via water vortex-driven piezo-activation for removing organic contaminants from water, *Environ. Sci. Ecotechnology*, 2022, **10**, 100165, DOI: 10.1016/J.ESE.2022.100165.

66 T. P. Farrell and R. B. Kaner, Conducting Polymers, *Encycl. Polym. Nanomater.*, 2013, 1–8, DOI: 10.1007/978-3-642-36199-9_2-1.

67 D. T. Oyekunle, X. Zhou, A. Shahzad and Z. Chen, Review on carbonaceous materials as persulfate activators: structure-performance relationship, mechanism and future perspectives on water treatment, *J. Mater. Chem. A*, 2021, **9**, 8012–8050, DOI: 10.1039/d1ta00033k.

68 J. Yu, H. Feng, L. Tang, Y. Pang, G. Zeng, Y. Lu, H. Dong, J. Wang, Y. Liu, C. Feng, J. Wang, B. Peng and S. Ye, Metal-free carbon materials for persulfate-based advanced oxidation process: Microstructure, property and tailoring, *Prog. Mater. Sci.*, 2020, **111**, 100654, DOI: 10.1016/j.pmatsci.2020.100654.


© 2024 The Author(s). Published by the Royal Society of Chemistry